Correlation between Photovoltaic Performance and Interchain-ordering Induced Delocalization of Electronics States in Conjugated Polymer Blends.

Naresh Chandrasekaran[abc], Eliot Gann[cf], Nakul Jain[b], Anshu kumar[d], Sreelekha Gopinathan[e], Aditya Sadhanla[g], Richard H. Friend[g], Anil Kumar[d], Christopher R. McNeill[c] and Dinesh Kabra[b*]*

Mr. N. Chandrasekaran

IITB-Monash Research Academy, IIT Bombay, Mumbai-400076, India.

Mr. N. Chandrasekaran, Mr. N. Jain, Prof. D. Kabra
Department of Physics, Indian Institute of Technology Bombay, Powai, Mumbai-400076, India.
dkabra@iitb.ac.in

Mr. N. Chandrasekaran, Dr. E. Gann, Prof. C. R. McNeill
Department of Materials Science and Engineering, Monash University, Wellington Road, Clayton, VIC 3800 Australia.
christopher.mcneill@monash.edu

Dr. A. Kumar, Prof. A. Kumar
Department of Chemistry, Indian Institute of Technology Bombay, Powai, Mumbai-400076, India.

Mrs S. P. Gopinathan,
Centre for Research in Nanotechnology & Science, Indian Institute of Technology Bombay, Powai, Mumbai-400076, India.

Dr. E. Gann.
Australian Synchrotron, 800 Blackburn Road, Clayton, VIC 3168 Australia.

Dr. Aditya Sadhanala and Prof. Richard H. Friend
Optoelectronics Group, Cavendish Laoratory, University of Cambridge, UK (CB3 0HE)

Abstract

In this paper we correlate the solar cell performance with bimolecular packing of donor:acceptor bulk heterojunction (BHJ) organic solar cells (OSCs), where interchain ordering of donor molecule and its influence on morphology, optical properties and charge carrier dynamics of BHJ solar cells is studied in detail. Solar cells that are fabricated using more ordered defect free 100% regioregular, poly(3-hexylthiophene) (DF-P3HT) as the donor polymer, shows ca. 10% increase in the average power conversion efficiency (PCE) when compared to the solar cell fabricated using 92% regioregularity P3HT, referred to as rr-P3HT. EQE and UV-Vis absorption spectrum shows clear increase in the 607 nm vibronic shoulder of DF-P3HT blend suggesting better interchain ordering which was also reflected in the less Urbach energy (E_u) value for this system. The increase in ordering inside the blend has enhanced the hole mobility which is calculated from the single carrier device J-V characteristics. Electroluminance (EL) studies on the DF-P3HT system showed a redshifted peak when compared to rr-P3HT-based devices suggesting low CT energy states in DF-P3HT. The morphology of the blend films are studied using AFM and Grazing-Incidence Wide-Angle X-ray Scattering (GIWAXS) suggesting increase in the roughness and phase segregation which could enhance the internal scattering of the light inside the device and improvement in the crystallinity along alkyl and π-stacking direction. Hence, higher PCE, Lower E_u, redshifted EL emission, high hole-mobility and better crystallinity suggest improved interchain ordering has facilitated more delocalized HOMO state in DF-P3HT based.

Keywords: Interchain order, Defect-free P3HT, charge carrier dynamics, morphology, organic solar cells.

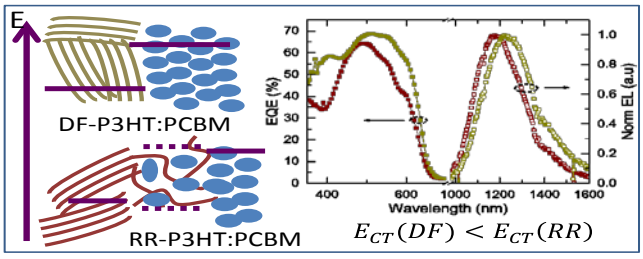

1. Introduction

P3HT is one of the most commonly used materials in organic electronics because of its simple synthesis and semi-crystalline lamellar microstructure.[1-2] It is a model system for synthetic chemist for the development of future low bandgap polymer systems that will be used in OPVs. P3HT:PCBM blends, in particular, have been extensively studied in the area of polymer solar cells[3-4], with PCEs reaching up to ~5%[5-6]; however, most studies report PCEs in the range of 3–4%.[7-9] Recent studies have achieved PCEs over 6% in polymer solar cells made up of P3HT and non-fullerene acceptor.[10] Despite high efficiency OPV reports from low bandgap polymers, polythiophene is still a model polymer system for synthetic chemist and for device physicist due to its unique structural and morphological properties in blend with acceptor molecules. OPV community still investigate P3HT polymer because of its simple synthesis route which has possibility of scaling up, whereas on the other hand, high performance low band gap polymers involve complex synthesis routes and scaling up of these polymers are challenging. These recent reports of over 6% PCE results are promising in making P3HT based solar cells more viable for commercial application. Most OPV cells/modules are being fabricated with inverted structure (n-i-p; relatively stable); this structure have nano-crystalline oxides film as an electron extracting layer and because of their rough surface a thick active layer is needed to overcome the pin-hole (shunts) issue in thin-film devices. Therefore, a relatively thicker photo-active material layer (without compromising much on charge transport, i.e., fill –factor and J_{sc}) in inverted structure can provide a good yield of high performance OPV cells.[11-12]

The nature of the donor polymer plays a vital role in the device performance of bulk heterojunction solar cells.[13] The variability in the device performance is also influenced by variations in polymer characteristics such as molecular weight, regioregularity, and polydispersity index (PDI).[14-16] The effect of different molecular weight of rr-P3HT upon the solar cell device performance and the charge mobility is discussed in detail by A. M. Ballantyne et al.[17] Increase in the molecular weight of rr-P3HT polymer has little influence on cell open circuit voltage and short circuit current, whereas fill-factor and charge (both hole and electron) mobility are reduced with increase in the molecular weight.[17] Poly-(3 alkylthiophenes) consists of a polythiophene backbone with alkyl side chains that are attached to the thiophene rings (**Figure 1a**). Since 3-alkylthiophene is not a symmetrical molecule, there are three relative orientations available when two 3-alkylthiophene rings are coupled between the 2- and 5- positions: 2-5’ or head-to-tail coupling (H-T), 2-2’ or head-to-

head coupling (H-H), and 5-5' or tail-to-tail coupling (T-T). P3HT synthesized with a mixture of these possible couplings is said to be irregular. Irregularly substituted polythiophenes have structures in which unfavorable H-H couplings cause a sterically driven twist of thiophene rings, resulting in a loss of conjugation. On the other hand, polymers that contain only head-to-tail (HT) couplings are denoted as regioregular. Regioregular P3HT can easily access a low energy planar conformation, leading to extended conjugation-length polymers.[18] For a 100% regioregular polymer chain, every 3-alkylthiophene unit is coupled with an H-T coupling. The introduction of any T-T or H-H couplings leads to defects, as shown in Figure 1a. It has been shown that the degree of regioregularity plays a vital role in improving the crystallinity and in increasing the device performance.[15-16, 19] Effect of regioregularity on bimolecular packing of P3HT:PCBM is studied using optical and structural studies in great detail by Kohn et al, which concluded that the structure is driven by the crystallization of the regioregular P3HT and forms ~ 10 nm structure domains of P3HT:PCBM.[20] The enhancement of device performance for higher regio-regularities is explained by improved conjugation length and π-π stacking, which facilitates charge transport in organic solar cells.[15-16] Although many studies have investigated the effect of regioregularity, few studies have utilized 100% regioregular (DF, termed as defect-free) P3HT.[21] Kim Y et al showed improvement in the polymer regioregularity (range of 90.7% to 95.2%) has a strong influence on the device performance.[16] However, the effect of 100% regioregular DF-P3HT on optical properties, charge carrier dynamics, morphology and photovoltaic performance has not yet been demonstrated. In this study we report the performance of P3HT:PCBM solar cells that are based on DF-P3HT and compare it to the performance of cells made from commercially available rr-P3HT. In addition to photovoltaic performance; optical properties, charge carrier dynamics and thin-film microstructure of P3HT:PCBM blends based on these materials are also compared and correlated with the device performance. DF-P3HT is prepared in-house with a Ni(0) based ex-situ initiator using one pot ex-situ Kumada Catalyst-Transfer Polymerization (KCTP) resulting in the synthesis of defect-free P3HT.[36] Interestingly, the NMR spectral investigations were found to be in agreement with previous report by Kohn et al and Senkovskyy et al.[21-22] A hallmark of quality of our DF-P3HT is 7-8 inch diameter shining sheet of P3HT film (see in Fig. 1c) with salient features of our approach are large scale batch-to-batch reproducibility and adaptability for continuous flow process, discussed elsewhere.

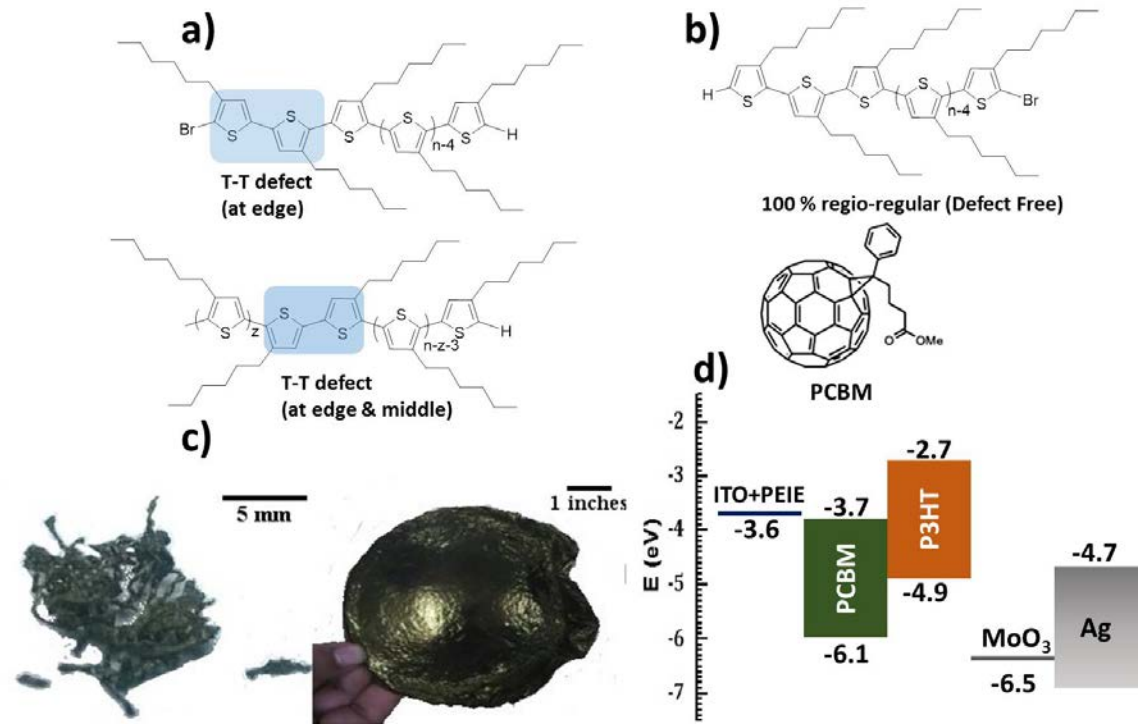

Figure 1: **a)** Represents the chemical structure of rr-P3HT with tail-tail (T-T) defect at the edge and at the middle of the polymer chain; **b)** The molecular structure of 100% regioregular DF-P3HT and PCBM; **c)** Images of rr (left) and DF (right) P3HT polymers; and **d)** Energy-level diagram of different layers in the solar cell.

2. Results and Discussion

2.1 Device parameters and optical studies

The device fabrication conditions are optimized for the DF-P3HT:PCBM and rr-P3HT:PCBM, resulting in an average PCE of 3.9 ± 0.4 and 3.5 ± 0.4, respectively for 16 devices. We observed that when the active layer thickness is ca. 130 nm, both DF-P3HT:PCBM and rr-P3HT:PCBM show similar performance (Table S1 in supporting information), but when the thickness of the active layer is increased to 230 nm, the performance of the DF-P3HT:PCBM cells is higher. In order to check whether changing the molecular weight (M_w) of the rr-P3HT affects the device performance, we fabricated solar cells using 75 kDa M_w rr-P3HT and obtained average PCE of 3.2 ± 0.4 for 16 devices.[37] This is in agreement with the previous study conducted by A.M. Ballantyne et al[17] werein increase in the M_w of P3HT results in decrease in FF of the device and also the performance. Since the performance of higher M_w rr-P3HT polymer is little less than 51 kDa rr-P3HT polymer, lower M_w rr-P3HT is used for comparison with DF-P3HT further in this study. The device

parameters of the best-performing cells are summarized in Table 1. The best device PCEs of 4.2% (DF) and 3.9 % (rr) are achieved. The J-V characteristics under AM 1.5G illumination and dark conditions are shown in **Figure 2(a)**. It is observed that the short circuit current density (J_{sc}) of devices fabricated using DF-P3HT:PCBM is ca. 20% higher than rr-P3HT:PCBM devices. The increase in the J_{sc} is also reflected in the EQE spectrum area of the DF-P3HT:PCBM device (Figure 2(b)). We also calculated the J_{sc} by integrating the EQE spectrum with the AM 1.5 spectrum and obtained a value of 10.1 and 8.1 mA/cm^2 for DF-P3HT and rr-P3HT devices, respectively. The reason for this discrepancy is attributed to edge-effects from the small cell active area of 0.045 cm^2.[23] In order to validate the shape of the EQE spectrum, we took the reflective absorption measurements on device structures by using a UV-Vis spectrometer with an integrating sphere. Figure 2(b) shows that the shape of the reflectance absorption spectrum matches well with the measured EQE spectra. The prominent shoulder at 607 nm is known to be attributed to the interchain transition in P3HT; the intensity of this shoulder correlated with the degree of interchain ordering.[24-26] The absorption by the extended conjugation length of the P3HT chain is attributed to the vibrionic shoulder at 558 nm.[27] Since the intensity of both of these peaks are enhanced in the DF-P3HT:PCBM device that leads to the increase in the area of EQE spectrum; one can conclude that the degree of interchain ordering and the conjugation length crystallinity of DF-P3HT is better when compared to the rr-P3HT based devices.[16] Figure 2(c) shows the EL spectra (normalized PL is shown in Fig. S1c) of these two devices. The PL emission from the blend is usually dominated by emission due to pure donor or acceptor materials and, here in our case, it is dominated by the P3HT PL emission with a trivial red shift observed in DF-P3HT:PCBM films. EL emissions that form OPVs, which comprise donor and acceptor material in the active medium, are attributed from the interfacial CT recombination.[28] From Figure 2(c), it is apparent that the peak EL emission of the DF-P3HT:PCBM device is ca. 30 meV redshifted when compared to the rr-P3HT:PCBM device, which has maximum peak EL emission at 1180 nm. This redshift in the EL emission can be attributed to the less energetic CT states that are present in the DF-P3HT:PCBM cells resulting from the better interchain ordering. The open circuit voltage (V_{oc}) of the OPV, which consists of donor and acceptor materials, is strongly correlated to the energy of the CT states,[28-30] and we attribute the decrease in V_{oc} and knee voltage (from dark curve) of DF-P3HT:PCBM cells to the less energetic CT state. The red shift in the EL emission is also attributed to molecular clustering and/or crystallization of materials.[28] Therefore, from this luminescence analysis we can conclude that DF-P3HT:PCBM cells have lower CT states than rr-P3HT:PCBM devices, and

the molecular clustering and/or crystallization is also high with lesser amorphous regions in DF-P3HT:PCBM films.[20-21] Hence, the HOMO level is broader, that is, delocalized with lesser tail states in the ordered DF-P3HT:PCBM blend than in the rr-P3HT:PCBM blend.

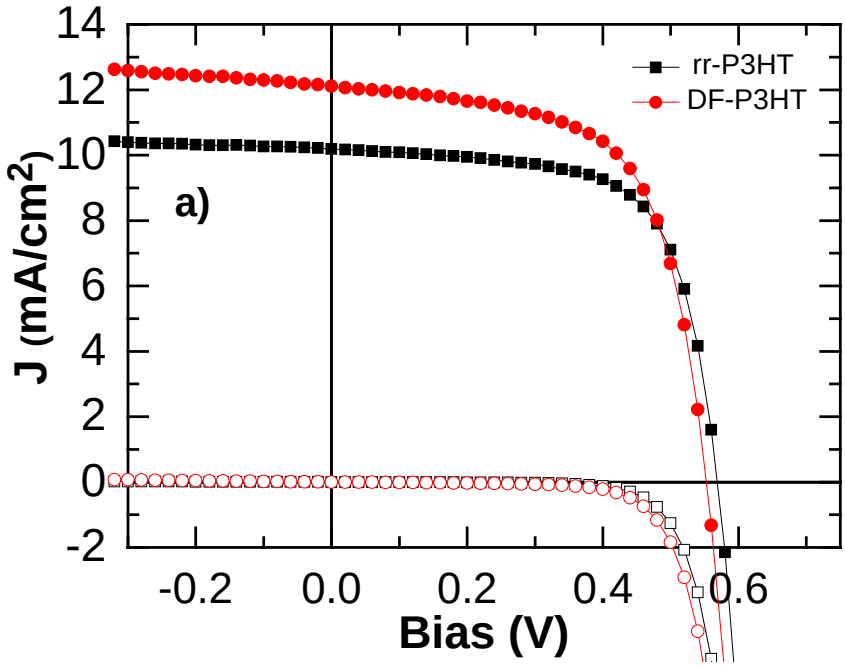

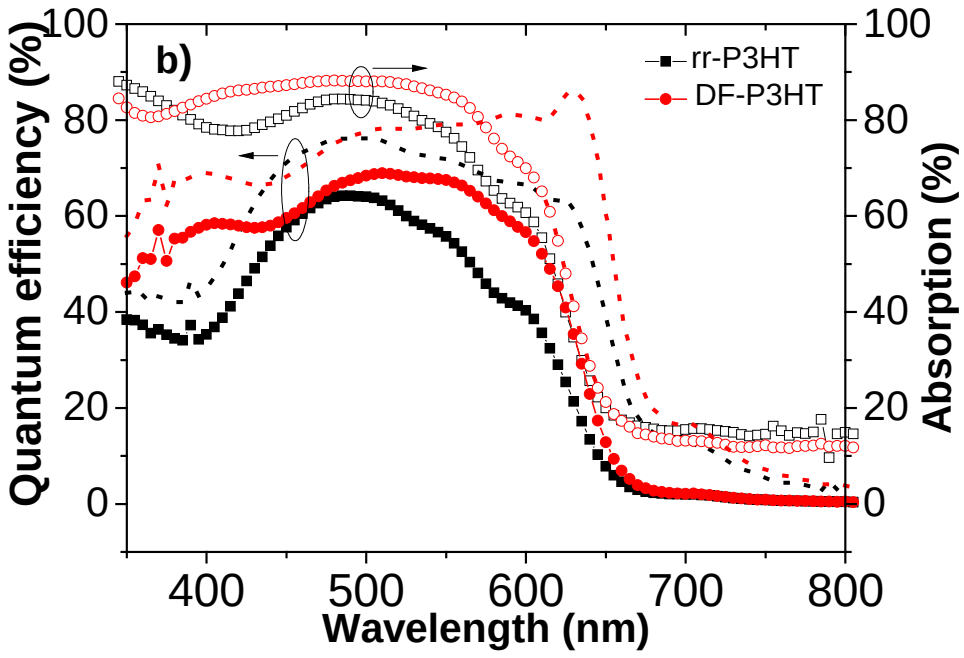

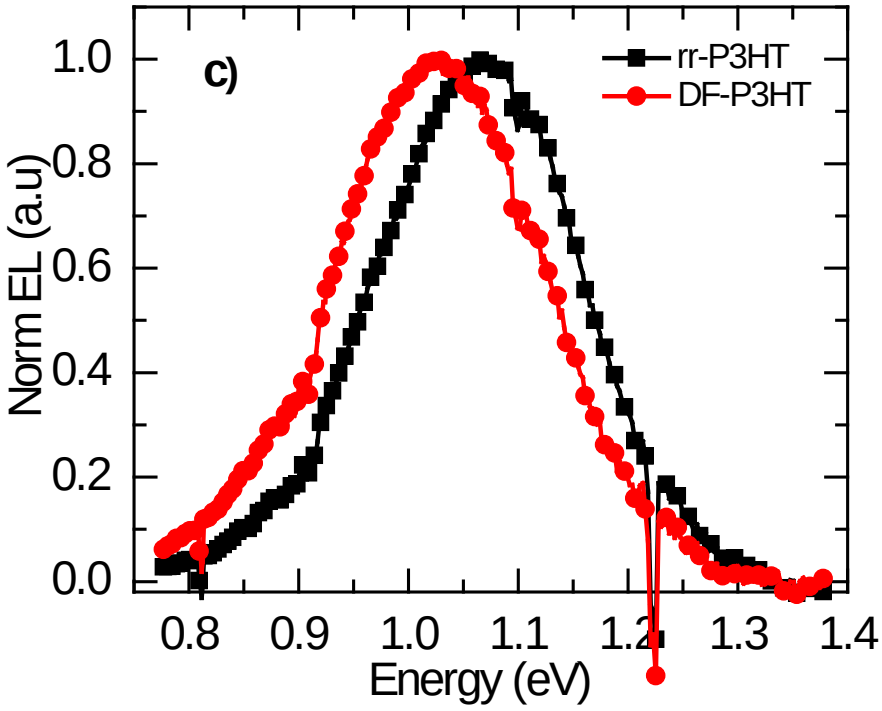

Figure 2: **a)** Dark (hollow) and lighted under AM 1.5G (solid) J-V characteristic; **b)** EQE spectrum of ITO/PEIE/activelayer/MoO_3/Ag solar cell using rr-P3HT:PCBM (square) and DF-P3HT:PCBM(circle) active layer. The dotted line represents the internal quantum efficiency, and the hollow plot represents the absorption percentage that is obtained from the reflection absorption measurement; and **c)** EL spectrum of rr-P3HT:PCBM and DF-P3HT:PCBM solar cells

Device	**J_{sc} (mA/cm^2)**	**V_{oc} (V)**	**FF (%)**	**PCE (%)**
rr-P3HT:PCBM-Mean	9.57	0.568	65.49	3.51 ± 0.37
rr-P3HT:PCBM-Best device	10.19	0.570	66.78	3.88
DF-P3HT:PCBM-Mean	11.21	0.554	62.21	3.85 ± 0.37
DF-P3HT:PCBM-Best device	12.11	0.553	63.06	4.22

Table 1: Summary of the mean of 16 devices and best device parameters of ITO/PEIE/active layer/MoO_3/Ag solar cell that is fabricated using rr and DF P3HTs.

2.1.1 Urbach Energy:

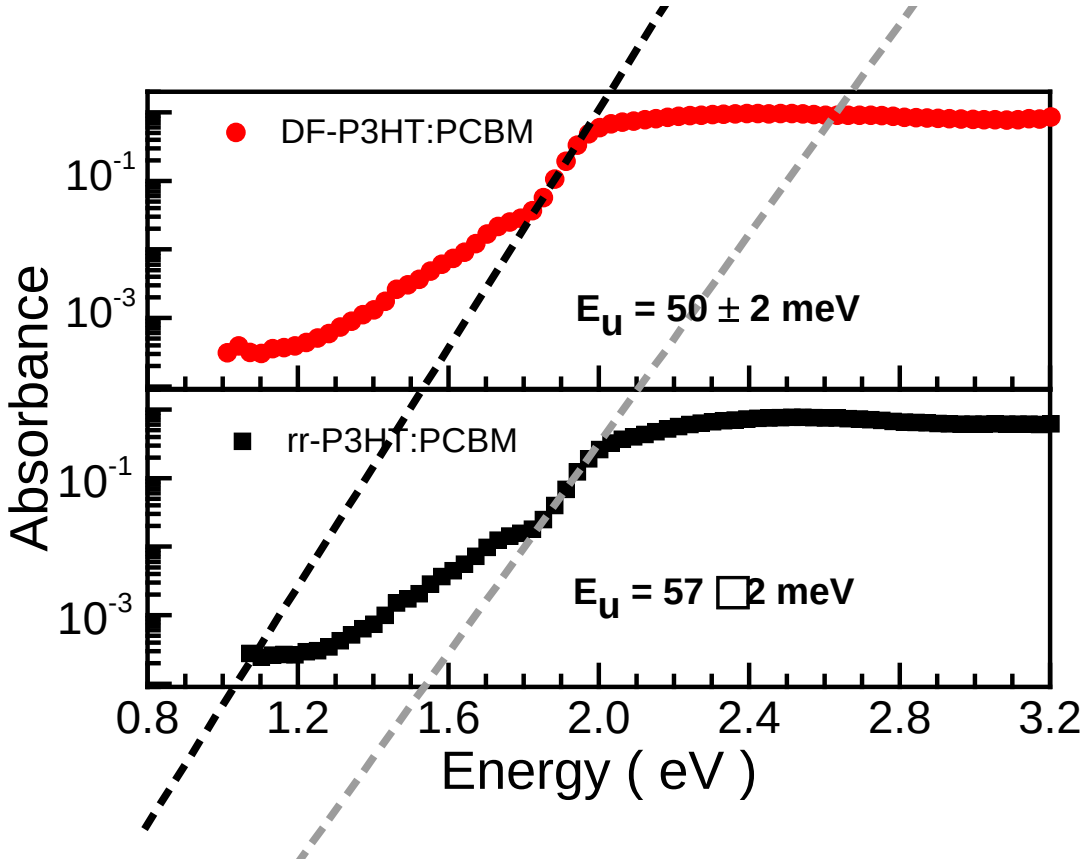

Figure 3: Absorbance as a function of photon energy of DF-P3HT:PCBM and rr-P3HT:PCBM blend films over quarts/PEIE substrate. The Urbach tails of these blends are fitted using a linear equation to obtain the Urbach energy (Eu).

Urbach energy is calculated from the absorbance vs photon energy plot shown in the **Figure 3** to determine the disorder present in these polymer blends. The absorbance beyond the band gap edge of the polymer is fitted with the linear equation to determine the slope, inverse of which give Urbach energy (E_u). We obtain Eu 57 ± 2 meV and 50 ± 2 meV for rr-P3HT:PCBM and DF-P3HT:PCBM blend films which were fabricated using the similar condition used during device fabrication. Eu is related to the disorder present in the material[31-32] and from the values obtained here we can conclude that DF-P3HT:PCBM blend has less disorder associated with it when compared to rr-P3HT:PCBM. This result is in support to our previous observations suggesting high regioregular P3HT is more ordered and better donor:acceptor bimolecular blend packing with lesser amount of amorphous regions of P3HT:PCBM.[20-21]

2.2 Charge transport properties of blend.

2.2.1 Single carrier devices:

The zero field mobility of these polymer blends are calculated by fitting the current-voltage curves of single carrier devices by using the Mott–Gurney equation $j = \frac{9}{8}\varepsilon\varepsilon_r\mu_0(\frac{(v-v_{bi})}{d^3})g\exp(\sqrt{v-v_{bi}})$. Where μ_0 is the zero field mobility, and d and v_{bi} are the thickness and built-in voltage inside the device. $g = \frac{\beta}{d}$ where the β field dependent parameter obtained from the fit. The ITO/MoO_3/P3HT:PCBM/Au structure was used to fabricate hole-only devices and the ITO/PEIE/P3HT:PCBM/ca/Al structure is used to fabricate electron-only devices. The hole mobility was found to be 3.36 × 10^{-7} m^2/Vs and 9.48 × 10^{-7} m^2/Vs for rr-P3HT:PCBM and DF-P3HT:PCBM, respectively. The zero field electron mobility for both these devices are, similarly, in the range of 1 × 10^{-6} m^2/Vs. The different thickness electron only and hole only devices J-V characteristics with Mott-Gurney fits are shown in Figure S5 and Figure S5 supporting information, respectively. The parameters extracted from the fit for the different thickness hole-only device is summarized in the **Table 2**. This increase in the hole mobility of DF-P3HT:PCBM is attributed to the enhancement in the degree of interchain ordering and an increase in the crystallinity of polymer chains, which results in phase-segregated donor and acceptor domains with a relatively higher delocalized HOMO level for DF-P3HT than rr-P3HT-based blend system. Interestingly, we note that despite having higher M_w for DF-P3HT (88K) we observe high hole mobility and better device performance which is contradiction to what Feng Liu et al. has observed.[33] We attribute this difference in trend to the good quality (high regioregularity and low PDI) of the P3HT in DF-P3HT system, which might compensate for high M_w by keeping chains extended (or unfolded) ends.[20-21] This results in good charge transport properties, i.e., FF of solar cells even at high Mw.

Device	Thickness (nm)	Mobility (m^2/V-s)	Beta (β)
rr-P3HT:PCBM	115	1.90 × 10^{-07}	-1.46 × 10^{-04}
rr-P3HT:PCBM	165	2.70 × 10^{-07}	-2.07 × 10^{-04}
rr-P3HT:PCBM	235	5.49 × 10^{-07}	-4.05 × 10^{-04}
DF-P3HT:PCBM	130	1.41 × 10^{-06}	-3.10 × 10^{-05}
DF-P3HT:PCBM	175	5.90 × 10^{-07}	-2.23 × 10^{-05}
DF-P3HT:PCBM	240	8.44 × 10^{-07}	-2.95 × 10^{-04}

Table 2: Parameters extracted by the fit by using the Mott–Gurney equation for hole-only devices.

2.3 Morphology

We investigate the surface morphology of these blend films using AFM, shown in **Figure 4**. There is a clear change in the morphology of the DF-P3HT:PCBM and rr-P3HT:PCBM blend films. The donor and acceptor domain size in the DF-P3HT:PCBM appears to be larger and coarser when compared to the rr-P3HT:PCBM films, which appear to be more intermixed and smooth. This increase in the domain size could facilitate the separation and collection of carriers, although an increased domain size could also result in reduced exciton dissociation efficiency. An increase in the degree of crystallinity could explain the increase in the surface roughness of the DF-P3HT:PCBM films. The AFM results also support the previous red shift in the EL measurement, confirming the molecular clustering and/or increase in the crystallinity in the DF-P3HT: PCBM cells, which results in more rough films. Along with the enhancement in optical absorption at the vibronic shoulder at 607 nm due to enhancement in the interchain packing and crystallinity of the polymer, the rough surface of the DF-P3HT:PCBM films could also enhance the internal scattering of the light inside the device and help in increasing the number of excitons generated from the incident light. In order to verify this, we measure the incident light absorption percentage inside DF-P3HT:PCBM and rr-P3HT:PCBM devices that have similar active layer thicknesses by using reflection absorption measurements. The reflective absorption spectra of the different P3HT devices are shown in the hollow plot of Figure 2b). It is evident from the plots that the DF-P3HT:PCBM device has more light absorption, from ~400 nm to ~620 nm wavelengths, when compared to the rr-P3HT:PCBM devices. We also calculated the internal quantum efficiency (IQE) using the formula $= \frac{EQE}{Absorbed\ photons\ (from\ reflective\ absorption\ measurement)}$. From Figure 2(b), the IQE of DF-P3HT:PCBM is seen to be higher than the rr-P3HT:PCBM cells, which is in agreement with other spectroscopy measurement. This confirms that the increased crystallinity not only enhances absorption at the vibrionic shoulder but that the surface roughness enhances the light absorption and the number of excitons generated in the DF-P3HT:PCBM solar cells.

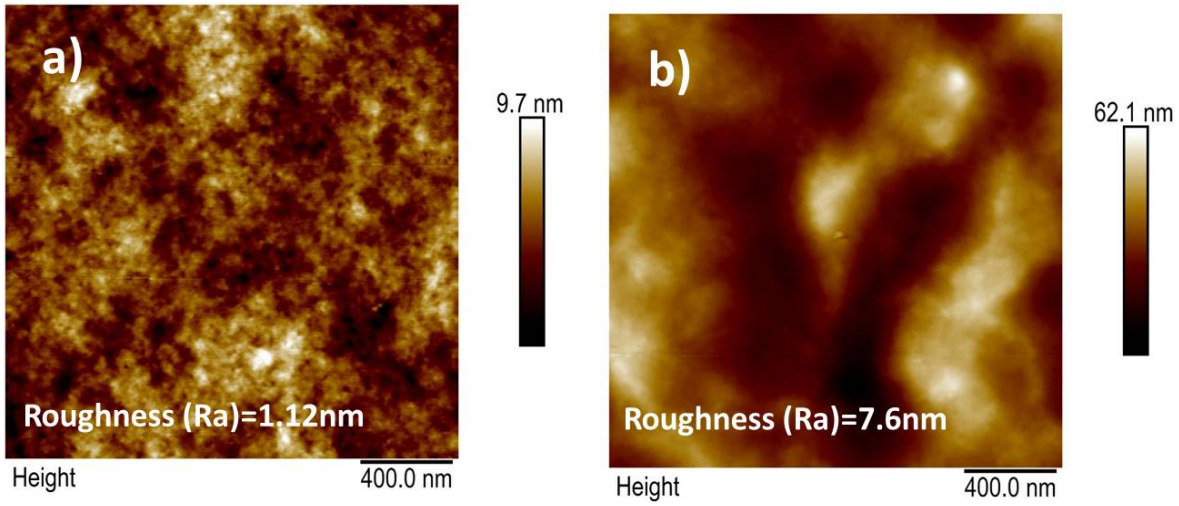

Figure 4. AFM images of **a)** ITO/PEIE/rr-P3HT:PCBM film; and **b)** ITO/PEIE/DF-P3HT:PCBM films annealed. Both rr and DF P3HT:PCBM films are annealed at 150 ℃ for ten minutes.

2.3.1 Microstructure:

We also performed Grazing-Incidence Wide-Angle X-ray Scattering (GIWAXS) to examine the crystalline morphology in these films, which reveal the packing distance, coherence lengths and orientation of the crystalline portions of the thin film, along with a general comparison of overall crystallinity between different films. The GIWAXS 2D scattering patterns of the films are shown in the supporting information Figure S7 along with the detail description of the experiment. The parameters calculated from the scattering profile are shown in the **Table 3**.

P3HT	d_{alk}	ξ_{alk}	I_{alk}	$d_{\pi-\pi}$	$\xi_{\pi-\pi}$	$I_{\pi-\pi}$
rr	1.696(1)	23.0(3)	104(1)	0.376(2)	8(2)	2.1(5)
DF	1.690(3)	16.0(7)	165(7)	0.377(1)	7(1)	5.5(7)

Table 3. Crystalline parameters determined by GIWAXS.

The unit cell appears unchanged between the two systems, with alkyl-stacking (100) distance (d_{alk}) of 1.7 nm and π-stacking (020) distance ($d_{\pi-\pi}$) of 0.377 nm for both systems. The coherence lengths ($\xi_{\pi-\pi}$) are essentially the same (~7 nm) in the electrically more important π-stacking direction. The largest difference between the two systems is the overall level of crystallinity in both the alkyl-stacking (I_{alk}) and the π-stacking ($I_{\pi-\pi}$) directions. The ratio of the amount of crystallinity in the DF system is ~1.5 times that in the rr system in the alkyl-stacking direction, and more than 2.5 times in the critical π-stacking direction.

Thus DF-P3HT polymer is more crystalline along the alkyl-stacking (I_{alk}) and the π-stacking ($I_{\pi-\pi}$) directions when compared to the 92% regioregular P3HT, both of which were fabricated at same condition. The increase in the crystallinity is also accompanied with decrease in disorder of the material which is evident from the Urbach energy measurements. This improvement in the material quality also resulted in red shift of EL emission. The enhanced absorption at the vibrionic shoulder and the roughness (internal scattering of light) of the film helps in increasing the incident light absorption inside the DF-P3HT:PCBM device. The increase in crystallinity also results in the high hole mobility in DF-P3HT:PCBM films when compared to the rr-P3HT:PCBM films. In addition to the above mentioned phenomenon enhancement in the interchain ordering induced crystallization helps in more free charge generation[34] but also compromising the device V_{oc} due to reduced diagonal bandgap ,i.e., CT state.

3. Conclusion

For the first time, we have fabricated solar cells with superior interchain packed Defect free (100% regioregular) P3HT. The device fabrication conditions were optimized for this polymer in order to reach a maximum power conversion efficiency of 4.2%. A comparative study was performed between best-performing DF-P3HT:PCBM and less interchain packed rr-P3HT:PCBM devices. It is evident from the EL spectra that the energy of CT states is lower in DF-P3HT:PCBM, which explains the lower knee voltage and V_{oc} in dark and illuminated J-V curves. The rough surface morphology and enhancement in the degree of ordering in the DF-P3HT:PCBM film explains the increase in the value and area of the DF-P3HT:PCBM EQE spectrum. The increase in the hole mobility of DF-P3HT:PCBM devices helps in extracting the charges faster when compared to rr-P3HT:PCBM devices. The relative crystallinity of DF-P3HT:PCBM and rr-P3HT:PCBM films is calculated from the GIWAXS data, and it is found that the overall fraction of crystallinity in DF-P3HT:PCBM is 1.5 time higher than that in rr-P3HT:PCBM, and more than two times higher along the alkyl and π-stacking directions, respectively. Thus, the increased interchain ordering and better bimolecular packing in the DF-P3HT which is due to the better quality (100% regioregularity and low PDI) P3HT leads to increased crystallinity, lower CT states, improved phase separation, increase hole mobility, and improved optical absorption, which explains the superior performance of DF-P3HT:PCBM devices when compared to rr-P3HT:PCBM devices. We believe that further device engineering with the DF-P3HT helps in achieve higher PCEs. High performance devices with thicker polymer films are susceptible to

inherent roughness of transparent conducting oxides, which supports higher yield of working devices for upcoming OPV technology.

4. Methodology

The solvents and materials were obtained from Sigma Aldrich and were used as received unless otherwise mentioned. Inverted solar cells with architecture ITO/PEIE/P3HT:PCBM/MoO_3/Ag were fabricated. ITO-coated glass substrates procured from Lumtec (sheet resistance 7Ω/sqr) were cleaned by ultra-sonicating with acetone and an IPA solution consecutively, each for ten minutes. The ITO substrates were then treated with air-oxygen plasma at RF power 18 W for ten minutes. A thin layer of polyethyleneamine (PEIE) from a 0.4 wt% solution in a 2-methoxyethanol was coated over the ITO and cured at 110℃ for 10 min. The substrates were then transferred into an N_2-filled glove box (GB) for the spin coating of the active layer. Two polymer blend solutions were prepared: one with commercially available rr-P3HT (Rieke Metals 4002-E) with molecular weight (M_w) and a PDI of 51kDa and 2.4, respectively, and the other with the DF-P3HT synthesized as per the procedure described by A.Kumar and coworkers.[36] Molecular weight was determined using Gel Permeation Chromatography with THF as mobile phase against polystyrene as standard. DF-P3HT with molecular weight (M_w) of 88kDa and PDI of 1.6 was used in this study. PCBM, which was purchased from Nano C (Westwood, MA) and used as the acceptor in both cases. The P3HT and PCBM with a weight ratio of 1:1 was dissolved in 1,2 dichlorobenzene (anhydrous 99%) at a concentration of 40mg/ml. The blend solution was spin-coated over the PEIE-coated ITO substrates. The spin-coating parameters were optimized to achieve the best performance in both the DF and rr-P3HT:PCBM devices. The substrates were annealed at 150°C for 10 min before deposition of the top electrodes. The hole extraction layer MoO_3 (15nm) and silver metal layer (100nm) were thermally evaporated at a pressure of $7x10^{-7}$ mbar inside a vacuum chamber that was integrated within the GB. The devices were encapsulated inside the GB with the Devcon 2-Ton Epoxy resin and taken out for characterization.

Dark and light current-voltage (J-V) characteristics of the solar cells were measured with a Keithley 2365 source meter. Simulated sunlight (100 mW/cm^2AM 1.5G) was provided by a Photo Emission Tech model SS50AAA solar simulator. The light intensity of the solar simulator was calibrated with a calibrated silicon photodiode with a KG3 filter before the measurement. External quantum efficiency (EQE) was measured with a tungsten lamp

(Newport 250 W QTH) as the light source dispersed through an Oriel Cornerstone 130 monochromator. The intensity of the light used in the EQE measurement was less than 1 mW/m^2, and effort was taken to ensure that the spot size was smaller than the active area of the device. The spectral mismatch between solar simulator lamp and AM1.5 spectrum with respect to the P3HT:PCBM cell response was found to be ca. 0.99. Reflectance absorption measurements were carried out on glass/PEIE/P3HT:PCBM/MoO_3/Ag samples. The samples were fabricated under conditions that were similar to those during the fabrication of the device. The reflectance spectrum was collected using an integrating sphere with a Lambda 950 spectrophotometer from PerkinElmer. For electroluminescence (EL) measurements, the device was excited using an electrical pulse of a height of 4V. A liquid nitrogen-cooled InGaAs array detector in conjunction with the Acton SP2300 spectrometer was used to collect the light that was emitted from the device. For Photoluminescence (PL) studies, the samples were excited using 532 nm laser, and the emission from the sample was collected using a Shamrock SR-303i spectrograph with Andor I-star grated ICCD. The surface morphology studies were carried out with a Veeco Nanoscope Vatomic force microscope (AFM) that used the scanAsyst mode.

Photothermal Deflection Spectroscopy (PDS) is a highly sensitive surface averaged absorption measurement technique. For the measurements, a monochromatic pump light beam produced by a combination of a Light Support MKII 100 W Xenon arc source and a CVI DK240 monochromator, is shone on the sample (thin-film on Quartz substrate), inclined perpendicular to the plane of the sample, which on absorption produces a thermal gradient near the sample surface via non-radiative relaxation induced heating. This results in a refractive index gradient in the area surrounding the sample surface. This refractive index gradient is further enhanced by immersing the sample in a deflection medium comprising of an inert liquid FC-72 Fluorinert® (3M Company) which has a high refractive index change per unit change in temperature. A fixed wavelength CW transverse laser probe beam, produced using a Qioptiq 670 nm fiber-coupled diode laser with temperature stabilizer for reduced beam pointing noise, was passed through the thermal gradient in front of the sample producing a deflection proportional to the absorbed light at that particular wavelength, which is detected by a differentially amplified quadrant photodiode and a Stanford Research SR830 lock-in amplifier combination. Scanning through different wavelengths gives us the complete absorption spectra.

Grazing-Incidence Wide-Angle X-ray Scattering (GIWAXS) measurements were taken at Australian Synchrotron at the SAXS/WAXS beamline.[35] The films were deposited over the silicon substrate, with the parameters closely matching the device fabrication, and achieved an active layer thickness of 230 nm. Photons of an energy level of 9 KeV were used, and 2D scattering patterns were recorded on a Pilatus 1M detector. The distance between the sample and the detector was calibrated using a silver behenate scattering standard. The angle of incidence of the X-rays is close to that of the polymer critical angle but below the critical angle of the silicon substrate, this is to ensure a minimal background signal from the substrate and a highly increased X-ray electric field intensity within the thin polymer film, which greatly increases the scattering intensity. The polymer films were exposed to the X-rays for three seconds in order to ensure that the films were not damaged. The diffraction data are expressed as a function of the scattering vector q, which has a magnitude of $(4\pi/\lambda)\sin(\theta)$, where θ is half the scattering angle and λ is the wavelength of the incident radiation.

Acknowledgements

GIWAXS measurements were undertaken at the SAXS/WAXS beamline at the Australian Synchrotron, Victoria, Australia. AFM studies were performed at the Melbourne Centre for Nanofabrication (MCN) in the Victorian Node of the Australian National Fabrication Facility (ANFF). We acknowledge DST (SB/S3/ME/037/2014) for funds and CEN & NCPRE IITB for device fabrication & characterizations, respectively. NC acknowledges the IITB-Monash Research Academy for the fellowship. AS and RHF would like to acknowledge the support from EPSRC and the India-UK APEX project.

References:

1. Frontmatter. In *Handbook of Oligo- and Polythiophenes*, Wiley-VCH Verlag GmbH: **2007**, pp i-xxiv.
2. Wong, W. S.; Salleo, A., *Flexible electronics: materials and applications*. Springer Science & Business Media: **2009**; Vol. 11.
3. Ng, A.; Liu, X.; Jim, W. Y.; Djurišić, A. B.; Lo, K. C.; Li, S. Y.; Chan, W. K., P3HT : PCBM solar cells—The choice of source material. *Journal of Applied Polymer Science* **2014,** *131* (2), n/a-n/a.
4. Dang, M. T.; Hirsch, L.; Wantz, G., P3HT:PCBM, Best Seller in Polymer Photovoltaic Research. *Advanced Materials* **2011,** *23* (31), 3597-3602.
5. Reyes-Reyes, M.; Kim, K.; Carroll, D. L., High-efficiency photovoltaic devices based on annealed poly(3-hexylthiophene) and 1-(3-methoxycarbonyl)-propyl-1- phenyl-(6,6)C61 blends. *Applied Physics Letters* **2005,** *87* (8), 083506.

6. Kim, K.; Liu, J.; Namboothiry, M. A. G.; Carroll, D. L., Roles of donor and acceptor nanodomains in 6% efficient thermally annealed polymer photovoltaics. *Applied Physics Letters* **2007,** *90* (16), 163511.
7. Chen, S.-Y.; Yen, Y.-T.; Chen, Y.-Y.; Hsu, C.-S.; Chueh, Y.-L.; Chen, L.-J., Large scale two-dimensional nanobowl array high efficiency polymer solar cell. *RSC Advances* **2012,** *2* (4), 1314-1317.
8. Wang, T.; Pearson, A. J.; Lidzey, D. G.; Jones, R. A. L., Evolution of Structure, Optoelectronic Properties, and Device Performance of Polythiophene:Fullerene Solar Cells During Thermal Annealing. *Advanced Functional Materials* **2011,** *21* (8), 1383-1390.
9. Xiao, T.; Cui, W.; Anderegg, J.; Shinar, J.; Shinar, R., Simple routes for improving polythiophene: fullerene-based organic solar cells. *Organic Electronics* **2011,** *12* (2), 257-262.
10. Nielsen, C. B.; Holliday, S.; Chen, H.-Y.; Cryer, S. J.; McCulloch, I., Non-Fullerene Electron Acceptors for Use in Organic Solar Cells. *Accounts of Chemical Research* **2015,** *48* (11), 2803-2812.
11. Krebs, F. C., Fabrication and processing of polymer solar cells: A review of printing and coating techniques. *Solar Energy Materials and Solar Cells* **2009,** *93* (4), 394-412.
12. Vaynzof, Y.; Kabra, D.; Brenner, T. J. K.; Sirringhaus, H.; Friend, R. H., Recent Advances in Hybrid Optoelectronics. *Israel Journal of Chemistry* **2012,** *52* (6), 496-517.
13. Scharber, M. C.; Mühlbacher, D.; Koppe, M.; Denk, P.; Waldauf, C.; Heeger, A. J.; Brabec, C. J., Design Rules for Donors in Bulk-Heterojunction Solar Cells—Towards 10 % Energy-Conversion Efficiency. *Advanced Materials* **2006,** *18* (6), 789-794.
14. Chang, J.-F.; Clark, J.; Zhao, N.; Sirringhaus, H.; Breiby, D. W.; Andreasen, J. W.; Nielsen, M. M.; Giles, M.; Heeney, M.; McCulloch, I., Molecular-weight dependence of interchain polaron delocalization and exciton bandwidth in high-mobility conjugated polymers. *Physical Review B* **2006,** *74* (11), 115318.
15. Jiang, X. M.; Österbacka, R.; Korovyanko, O.; An, C. P.; Horovitz, B.; Janssen, R. A. J.; Vardeny, Z. V., Spectroscopic Studies of Photoexcitations in Regioregular and Regiorandom Polythiophene Films. *Advanced Functional Materials* **2002,** *12* (9), 587-597.
16. Kim, Y.; Cook, S.; Tuladhar, S. M.; Choulis, S. A.; Nelson, J.; Durrant, J. R.; Bradley, D. D. C.; Giles, M.; McCulloch, I.; Ha, C.-S.; Ree, M., A strong regioregularity effect in self-organizing conjugated polymer films and high-efficiency polythiophene:fullerene solar cells. *Nat Mater* **2006,** *5* (3), 197-203.
17. Ballantyne, A. M.; Chen, L.; Dane, J.; Hammant, T.; Braun, F. M.; Heeney, M.; Duffy, W.; McCulloch, I.; Bradley, D. D. C.; Nelson, J., The Effect of Poly(3-hexylthiophene) Molecular Weight on Charge Transport and the Performance of Polymer:Fullerene Solar Cells. *Advanced Functional Materials* **2008,** *18* (16), 2373-2380.
18. McCullough, R. D., The Chemistry of Conducting Polythiophenes. *Advanced Materials* **1998,** *10* (2), 93-116.
19. Sirringhaus, H.; Brown, P. J.; Friend, R. H.; Nielsen, M. M.; Bechgaard, K.; Langeveld-Voss, B. M. W.; Spiering, A. J. H.; Janssen, R. A. J.; Meijer, E. W.; Herwig, P.; de Leeuw, D. M., Two-dimensional charge transport in self-organized, high-mobility conjugated polymers. *Nature* **1999,** *401* (6754), 685-688.
20. Kohn, P.; Rong, Z.; Scherer, K. H.; Sepe, A.; Sommer, M.; Müller-Buschbaum, P.; Friend, R. H.; Steiner, U.; Hüttner, S., Crystallization-Induced 10-nm Structure Formation in P3HT/PCBM Blends. *Macromolecules* **2013,** *46* (10), 4002-4013.
21. Kohn, P.; Huettner, S.; Komber, H.; Senkovskyy, V.; Tkachov, R.; Kiriy, A.; Friend, R. H.; Steiner, U.; Huck, W. T. S.; Sommer, J.-U.; Sommer, M., On the Role of Single Regiodefects and Polydispersity in Regioregular Poly(3-hexylthiophene): Defect Distribution, Synthesis of Defect-Free Chains, and a Simple Model for the Determination of Crystallinity. *Journal of the American Chemical Society* **2012,** *134* (10), 4790-4805.

22. Senkovskyy, V.; Sommer, M.; Tkachov, R.; Komber, H.; Huck, W. T. S.; Kiriy, A., Convenient Route To Initiate Kumada Catalyst-Transfer Polycondensation Using Ni(dppe)Cl2 or Ni(dppp)Cl2 and Sterically Hindered Grignard Compounds. *Macromolecules* **2010,** *43* (23), 10157-10161.
23. Li, Z.; Gao, F.; Greenham, N. C.; McNeill, C. R., Comparison of the Operation of Polymer/Fullerene, Polymer/Polymer, and Polymer/Nanocrystal Solar Cells: A Transient Photocurrent and Photovoltage Study. *Advanced Functional Materials* **2011,** *21* (8), 1419-1431.
24. Li, L.; Lu, G.; Yang, X., Improving performance of polymer photovoltaic devices using an annealing-free approach via construction of ordered aggregates in solution. *Journal of Materials Chemistry* **2008,** *18* (17), 1984-1990.
25. Brown, P. J.; Thomas, D. S.; Köhler, A.; Wilson, J. S.; Kim, J.-S.; Ramsdale, C. M.; Sirringhaus, H.; Friend, R. H., Effect of interchain interactions on the absorption and emission of poly(3-hexylthiophene). *Physical Review B* **2003,** *67* (6), 064203.
26. Gurau, M. C.; Delongchamp, D. M.; Vogel, B. M.; Lin, E. K.; Fischer, D. A.; Sambasivan, S.; Richter, L. J., Measuring Molecular Order in Poly(3-alkylthiophene) Thin Films with Polarizing Spectroscopies. *Langmuir* **2007,** *23* (2), 834-842.
27. Kiriy, N.; Jähne, E.; Adler, H.-J.; Schneider, M.; Kiriy, A.; Gorodyska, G.; Minko, S.; Jehnichen, D.; Simon, P.; Fokin, A. A.; Stamm, M., One-Dimensional Aggregation of Regioregular Polyalkylthiophenes. *Nano Letters* **2003,** *3* (6), 707-712.
28. Tvingstedt, K.; Vandewal, K.; Gadisa, A.; Zhang, F.; Manca, J.; Inganäs, O., Electroluminescence from Charge Transfer States in Polymer Solar Cells. *Journal of the American Chemical Society* **2009,** *131* (33), 11819-11824.
29. Vandewal, K.; Gadisa, A.; Oosterbaan, W. D.; Bertho, S.; Banishoeib, F.; Van Severen, I.; Lutsen, L.; Cleij, T. J.; Vanderzande, D.; Manca, J. V., The Relation Between Open-Circuit Voltage and the Onset of Photocurrent Generation by Charge-Transfer Absorption in Polymer : Fullerene Bulk Heterojunction Solar Cells. *Advanced Functional Materials* **2008,** *18* (14), 2064-2070.
30. Veldman, D.; Meskers, S. C. J.; Janssen, R. A. J., The Energy of Charge-Transfer States in Electron Donor–Acceptor Blends: Insight into the Energy Losses in Organic Solar Cells. *Advanced Functional Materials* **2009,** *19* (12), 1939-1948.
31. Kurik, M. V., Urbach rule. *physica status solidi (a)* **1971,** *8* (1), 9-45.
32. Venkateshvaran, D.; Nikolka, M.; Sadhanala, A.; Lemaur, V.; Zelazny, M.; Kepa, M.; Hurhangee, M.; Kronemeijer, A. J.; Pecunia, V.; Nasrallah, I.; Romanov, I.; Broch, K.; McCulloch, I.; Emin, D.; Olivier, Y.; Cornil, J.; Beljonne, D.; Sirringhaus, H., Approaching disorder-free transport in high-mobility conjugated polymers. *Nature* **2014,** *515* (7527), 384-388.
33. Liu, F.; Chen, D.; Wang, C.; Luo, K.; Gu, W.; Briseno, A. L.; Hsu, J. W. P.; Russell, T. P., Molecular Weight Dependence of the Morphology in P3HT:PCBM Solar Cells. *ACS Applied Materials & Interfaces* **2014,** *6* (22), 19876-19887.
34. Bakulin, A. A.; Rao, A.; Pavelyev, V. G.; van Loosdrecht, P. H. M.; Pshenichnikov, M. S.; Niedzialek, D.; Cornil, J.; Beljonne, D.; Friend, R. H., The Role of Driving Energy and Delocalized States for Charge Separation in Organic Semiconductors. *Science* **2012,** *335* (6074), 1340-1344.
35. Kirby, N. M.; Mudie, S. T.; Hawley, A. M.; Cookson, D. J.; Mertens, H. D. T.; Cowieson, N.; Samardzic-Boban, V., A low-background-intensity focusing small-angle X-ray scattering undulator beamline. *Journal of Applied Crystallography* **2013,** *46* (6), 1670-1680.

36. Dattatray L. Tarange, Sreelekha Gopinathan, Anshu Kumar, Anil Kumar, *Communicated*

37. Naresh Chandrasekaran, Anil Kumar, Chris McNeill, Dinesh Kabra, *Communicated*.